Meccanica (2015) 50:2487–2496
DOI 10.1007/s11012-015-0146-8

Real-time displacement monitoring of a composite stiffened panel subjected to mechanical and thermal loads

Priscilla Cerracchio · Marco Gherlone · Alexander Tessler

Received: 13 January 2015 / Accepted: 6 March 2015 / Published online: 24 March 2015

Abstract Real-time reconstruction of the deformed structural shape using in situ strain measurements is an inverse problem, commonly called *shape sensing*. The knowledge of the deformed structural shape in real time has important implications for assessing strain, stress, and failure states, and thus constitutes a key component of structural health monitoring. In addition, shape sensing is required for control and actuation of smart structures. In this paper, shape sensing analyses are carried out for typical composite stiffened structures using the inverse Finite Element Method (iFEM). By using a limited set of discrete strain data, iFEM allows full-field reconstruction of displacements that can thus be monitored also far from sensor locations. First, the iFEM theoretical framework and the formulation of a triangular, inverse shell element are briefly discussed. Then, a general strain-sensor configuration amenable to stiffened shell structures is proposed. Several numerical results are presented for static, dynamic, and thermal loadings. The robustness of the method with respect to input errors is also investigated. It is shown that iFEM is a viable methodology for shape sensing of composite stiffened structures, having the desired computational efficiency, accuracy, and robustness with respect to strain-measurement errors. The iFEM shape-sensing methodology is particularly attractive because it does not require any information regarding applied loading, elastic material constants, inertial properties, or damping characteristics.

Keywords Shape sensing · Inverse Finite Element Method · Composite stiffened panel

P. Cerracchio (✉) · M. Gherlone
Department of Mechanical and Aerospace Engineering, Politecnico di Torino, Corso Duca degli Abruzzi 24, 10129 Turin, Italy
e-mail: priscilla.cerracchio@polito.it

M. Gherlone
e-mail: marco.gherlone@polito.it

A. Tessler
Structural Mechanics and Concepts Branch, NASA Langley Research Center, Mail Stop 190, Hampton, VA 23681-2199, USA
e-mail: Alexander.tessler-1@nasa.gov

1 Introduction

Substantial advances in composites technology over the past several decades have led to an increased use of laminated composite structures in civilian and military aircraft, aerospace vehicles, and naval ships. In particular, composite stiffened panels are widely used in airframe structures, due to their high stiffness-to-weight and strength-to-weight ratios, durability and tailoring freedom. A major drawback of composite laminates is that damage due to impact, which is commonly invisible, may affect significantly the load-carrying structural capacity [1–4]. Traditional non-destructive techniques are time-consuming, costly and

often impractical for real-time response in large-scale structures [5]. For these reasons, the development of integrated Structural Health Management systems attracted much attention in recent years, for the purpose of increasing safety and reducing maintenance cost [6–9].

The monitoring of a structural system is traditionally performed with a network of bonded or embedded strain sensors. Many damage detection techniques have been proposed in the literature, which aim at indentifying structural damages by using a large amount of strain data [10]. The major difficulties of these kind of techniques reside in the ability to identify defects at a very early stage and also far from sensor locations. In other works, strain data recorded on a network of strain sensors have been used to predict the impact locations [11, 12]. Further actions are then needed to determine whether the structure is damaged or not. More efficiently, strains measured in real time at discrete sensor locations can be used to extrapolate strain data throughout the whole structure. This is commonly achieved through the estimation of the deformed structural shape.

Known as *shape sensing*, the reconstruction of the deformed shape from strain data enables the full-field reconstruction of structural strains and stresses, and the application of failure criteria for structural health assessment. The possibility to detect structural damages by using different shape sensing approaches was also investigate by Quach et al. [13] and by Derkevorkian et al. [14]. Shape sensing technologies are particularly attractive when it is difficult to determine or measure applied loads such as aerodynamic forces, vibrating excitations transmitted through junctions or impact loads. In these cases, knowledge of actual stress state allows failure prediction and cost-efficient maintenance to be performed based on actual data. It is worth pointing out that monitoring of the deformed shape is also a key aspect in the development of smart structures, such as those with morphing capabilities or structures with embedded antenna arrays. Such structures require real-time shape sensing to provide feedback to the actuation and control systems [15, 16].

Most of the existing shape sensing methods in the literature are restricted to slender beams or thin plates by virtue of the kinematic assumptions. Ko et al. [17] proposed a one-dimensional scheme based on classical beam theory to evaluate the deflection and cross-sectional twist angle of an aircraft wing. Using a two-line strain-sensing system on the top surface of the wing, the curvature is obtained at discrete locations along the wing span, by knowing the axial surface strain and the distance of the measuring device from the neutral axis. Then the deflection is evaluated by numerical integration at the two sensing lines only. The cross-sectional twist angle is computed by considering the difference in the deflection of the two lines. Other methods based on the classical bending assumptions define the bending curvature using an a priori set of basis functions and proper weights that are determined by strain–displacement relationships and measured surface strains [18–21]. For example, Jones et al. [20] reconstructed plate deflections by fitting in a least-squares sense discrete measures of the bending curvatures and by integrating the regression curves. Glaser et al. [21] used piecewise basis functions to fit experimental estimates of the curvature and to evaluate the deformed shape of a beam subjected to bending loads. The aforementioned methods rely on the selection of proper basis functions or fitting polynomials and therefore are not general enough to accommodate complex structural topologies and boundary conditions (e.g., built-up airframe structures).

Foss and Haugse [22], and Pisoni et al. [23] proposed a modal transformation method that approximates the displacement field as linear combination of normal modes. The coefficients to assign to each mode are evaluated in a least-square sense from measured strains. In [22] and [23] the mode shapes were experimentally estimated. In [24], FEM generated mode shapes where used, thus requiring a detailed description of the elastic and inertial material properties, the kind of data that are either unavailable or difficult to obtain. Moreover, for high-frequency excitations a large number of natural vibration modes is needed to improve the accuracy, thus requiring a computationally intensive eigenvalue analysis [25, 26].

The method described in [17] does not enable the full-field displacement solution and thus it is not suited for the structural health monitoring. Methods based on the interpolation of the bending curvature [17–21] may become really inaccurate for problems where the transverse shear effect is not negligible. Moreover it is difficult to find proper fitting functions for tridimensional structures, such as a stiffened panel, that are

accurate under a wide range of loadings. Works [22–26] address also complex structures but require sufficiently accurate elastic-inertial material information.

Tessler and Spangler [27] developed a robust and computationally efficient methodology for the full-field reconstruction of displacements of plates and shells. The approach uses a least-squares variational principle that accounts for the stretching, bending, and transverse shear deformations that correspond to first-order shear deformation theory. The variational framework requires only a C^0-continuous discretization of the displacement field, resulting in an inverse Finite Element Method (iFEM) [28, 29]. Because only strain–displacement relations are used in the formulation, both static and dynamic response can be reconstructed without any a priori knowledge of material, inertial, loading, or damping structural properties. Recently, with the goal of analyzing an important class of space structures, Gherlone et al. [30] applied the iFEM variational framework to develop shear-deformable beam and frame inverse finite elements. Application of the beam-iFEM approach to experimentally measured strains has been presented by Gherlone et al. [31], who used relatively coarse iFEM discretizations to reconstruct the static and dynamic response of a cantilevered beam.

In this paper, a facet shell-element iFEM formulation is utilized to study its applicability for composite stiffened shell structures that are commonly used in the design of aerospace, naval and civil structures. The purposes are to verify the accuracy of the method for complex structures subjected to different types of loading and to provide guidelines for the design of a suitable iFEM model and strain-sensor configuration, for shape sensing of general stiffened structures. Moreover, the effect of thermal loading on the accuracy of the predicted displacements is studied for the first time.

2 Theoretical basis: inverse Finite Element Method

The inverse Finite Element Method (iFEM) is a robust and versatile methodology that allows the reconstruction of the deformed shape of a structure by using arbitrarily positioned strain sensors. Herein, the general iFEM methodology [27] is first briefly reviewed. Then, the formulation of a three-node, facet inverse-shell element, based on Mindlin theory [28, 29], is discussed.

2.1 Variational principle

Consider a discretization of the structural domain, Ω, using one-, two- or three dimensional finite elements to suit the particular structure to be analyzed. Using a Cartesian coordinate system $\mathbf{x} \equiv (x, y, z)$,the displacement vector $\{u_x(\mathbf{x}), u_y(\mathbf{x}), u_z(\mathbf{x})\}$ can be expressed in terms of a set of *kinematic variables* $\mathbf{u}(\mathbf{x})$ that are consistent with a particular structural theory. The kinematic variables are then interpolated by a set of suitable element-shape functions as.

$$\mathbf{u}(\mathbf{x}) \approx \mathbf{u}^e = N(\mathbf{x})\mathbf{q}^e \tag{1}$$

where $\mathbf{N}$ denotes the shape-function matrix and $\mathbf{q}^e$ the nodal degrees-of-freedom.

Depending on the selected theory the strain field is completely defined by a set of K independent terms, $\boldsymbol{\varepsilon} \equiv \{\varepsilon_k\}(k = 1, \ldots, K)$, commonly referred to as *strain measures*. The strain measures are expressed in terms of the nodal displacement degrees-of-freedom as.

$$\boldsymbol{\varepsilon}(\mathbf{u}^e) = \mathbf{B}(\mathbf{x})\mathbf{q}^e \tag{2}$$

where the matrix $\mathbf{B}$ contains the derivatives of the shape functions.

The iFEM displacement solution is obtained by minimizing an error functional defined as the least-squares error between the analytic strain measures, given by Eq. (2), and the corresponding experimental strains, $\boldsymbol{\varepsilon}^{\varepsilon} \equiv \{\varepsilon_k^{\varepsilon}\}(k = 1, \ldots, K)$, measured at n discrete locations by in situ strain gauges, rosettes, or other types of strain sensors. For a single element, the error functional is given by.

$$\Phi^e(\mathbf{u}^e) = \|\boldsymbol{\varepsilon}(\mathbf{u}^e) - \boldsymbol{\varepsilon}^{\varepsilon}\|^2 \tag{3}$$

where the element functional Φ^e is given by sum of the products of the least-squares component, Φ_k^e, referred to the k-th strain component, and the weighting coefficient, w_k^e,

$$\Phi^e(\mathbf{u}^e) \equiv \sum_k w_k^e \Phi_k^e \tag{4}$$

with Φ_k^e given as the Euclidean norm

$$\Phi_k^e \equiv \frac{1}{n}\sum_{i=1}^{n}\left[\varepsilon_{k(i)}(\mathbf{u}^e) - \varepsilon_{k(i)}^{\varepsilon}\right]^2 \quad (k = 1, \ldots K) \qquad (5)$$

The weighting coefficients w_k^e account for dimensional coefficients, which guarantee that the terms in Eq. (4) have the same mathematical units. Moreover, w_k^e may include dimensionless coefficients, λ_k^e, which may be assigned different values to enforce a stronger or weaker correlation between the measured strain-measure components and their analytic counterparts. Generally speaking, in a weighted least-square approach, the weighting coefficients determine how much the multiplied terms influence the final estimates. Thus, if terms related to certain strain measures are multiplied by larger values of λ_k^e than the others, the solution will be pulled toward matching these strain data, whereas the error committed on the other strain components will have little influence on the solution (refer to [29] and Sect. 2.2).

The element functional Φ^e is minimized with respect to the unknown nodal degrees-of-freedom, $\mathbf{q^e}$, yielding the element matrix equation $\mathbf{a}^e\mathbf{q}^e = \mathbf{b}^e$. Taking into account appropriate coordinate transformations, the element contributions are assembled into a global system of equations

$$\mathbf{Aq} = \mathbf{b} \qquad (6)$$

where the matrix $\mathbf{A}$ depends on the shape functions and strain-gauge locations, whereas the vector $\mathbf{b}$ incorporates the measured strain values. The matrix $\mathbf{A}$ is a well-conditioned square matrix. Thus, upon enforcement of problem-dependent displacement boundary conditions that prevent rigid-body motion, the unknown nodal displacements and rotations are efficiently computed from Eq. (6) by the vector–matrix multiplication, $\mathbf{q} = \mathbf{A}^{-1}\mathbf{b}$. Thus, for real time applications, $\mathbf{A}$ is inverted only once (assuming small displacements, and that the strain-sensor locations remain unchanged). The vector $\mathbf{b}$, however, needs to be updated at each strain-data acquisition increment.

Since only strain–displacement relationships are used in the formulation, the compatibility equations are automatically satisfied. Furthermore, the method does not require the knowledge of any material properties or the applied loading. Thus, it is applicable for both static and dynamic loading conditions, without requiring inertial or damping material properties.

2.2 Mindlin, triangular inverse element

Utilizing Mindlin plate theory, a three-node inverse plate element, labeled *iMIN3*, was developed in [28]. The element uses C^0-continous anisoparametric shape functions to resolve issues associated with shear locking in thin plates. The basic equations are summarized as follows.

Consider a plate of thickness $2t$ referred to a Cartesian coordinate system $\mathbf{x} \equiv (x, y, z)$, where (x, y) identify the mid-plane (Fig. 1). The components of the displacement vector are given as

$$\begin{aligned} u_x(\mathbf{x}) &= u + z\theta_y \\ u_y(\mathbf{x}) &= v + z\theta_x \\ u_z(\mathbf{x}) &= w \end{aligned} \qquad (7)$$

where u and v are the average uniform displacements in the x and y directions, respectively; θ_x and θ_y are the rotations of the normal about the negative x and positive y axes, respectively; and w is an average transverse deflection. The five kinematic variables are $\mathbf{u} \equiv \{u, v, w, \theta_x, \theta_y\}^T$. In [28], the deflection variable is interpolated with a quadratic polynomial, whereas the other four kinematic variables vary linearly over the element. By using the anisoparametric interpolations described in [28], truly thin plates can be modeled without incurring excessive stiffening due to shear locking and the resulting element has the same number of degrees-of-freedom as a standard linear-interpolation element.

Invoking Mindlin theory, the strain field is identified by eight strain measures, $\{\varepsilon_k\} = \{\mathbf{e}, \mathbf{k}, \mathbf{g}\}^T$ $(K = 8)$, given by

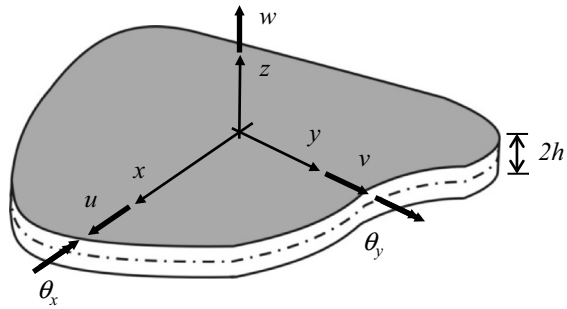

Fig. 1 Plate notation

$$\begin{aligned}\mathbf{e} &= \left\{u_{,x},\, v_{,y},\, \theta_{x,y}+\theta_{y,x}\right\}^T = \left\{\varepsilon_1,\, \varepsilon_2,\, \varepsilon_3\right\}^T \\ \mathbf{k} &= \left\{\theta_{y,x},\, \theta_{x,y},\, \theta_{x,x}+\theta_{y,y}\right\}^T = \left\{\varepsilon_4,\, \varepsilon_5,\, \varepsilon_6\right\}^T \\ \mathbf{g} &= \left\{w_{,x}+\theta_y,\, w_{,y}+\theta_x\right\}^T = \left\{\varepsilon_7,\, \varepsilon_8\right\}^T\end{aligned} \tag{8}$$

which define the *membrane* (**e**), *bending* (**k**) and *transverse-shear* (**g**) deformations.

To enable application of Eq. (3), the strain measures have to be experimentally evaluated from strain-sensor data. The strain measures $\mathbf{e}^{\varepsilon}_{(i)}$ and $\mathbf{k}^{\varepsilon}_{(i)}$ can be easily evaluated at discrete locations $(x, y)_i$ $(i = 1, \ldots, n)$ from surface strains measured on the top (+) and bottom (−) surfaces (see Fig. 2) as

$$\begin{aligned}\mathbf{e}^{\varepsilon}_i &\equiv \left\{\begin{array}{c}\varepsilon^{\varepsilon}_{x0}\\ \varepsilon^{\varepsilon}_{y0}\\ \gamma^{\varepsilon}_{120}\end{array}\right\}_i = \frac{1}{2}\left(\left\{\begin{array}{c}\varepsilon^{+}_{11}\\ \varepsilon^{+}_{22}\\ \gamma^{+}_{12}\end{array}\right\}_i + \left\{\begin{array}{c}\varepsilon^{-}_{11}\\ \varepsilon^{-}_{22}\\ \gamma^{-}_{12}\end{array}\right\}_i\right), \\ \boldsymbol{\kappa}^{\varepsilon}_i &\equiv \left\{\begin{array}{c}\kappa^{\varepsilon}_{10}\\ \kappa^{\varepsilon}_{20}\\ \kappa^{\varepsilon}_{120}\end{array}\right\}_i = \frac{1}{2h}\left(\left\{\begin{array}{c}\varepsilon^{+}_{11}\\ \varepsilon^{+}_{22}\\ \gamma^{+}_{12}\end{array}\right\}_i - \left\{\begin{array}{c}\varepsilon^{-}_{11}\\ \varepsilon^{-}_{22}\\ \gamma^{-}_{12}\end{array}\right\}_i\right)\end{aligned} \tag{9}$$

where $\{\varepsilon^{+}_{xx}, \varepsilon^{+}_{yy}, \gamma^{+}_{xy}\}_i$ and $\{\varepsilon^{-}_{xx}, \varepsilon^{-}_{yy}, \gamma^{-}_{xy}\}_i$ denote the in-plane surface strains measured respectively at $[(x, y)_i, +h]$ and $[(x, y)_i, -h]$. By using the present kinematic interpolations, the membrane strains and bending curvatures result to be constant across the element. This implies that one measurement point per element is sufficient and it would be optimally located at the element centroid.

The transverse shear strain measures **g** cannot be obtained experimentally. Thus, for the terms in the functional including the strain measures **g**, the L_2 norm is used ($k = 7, 8$) [27]

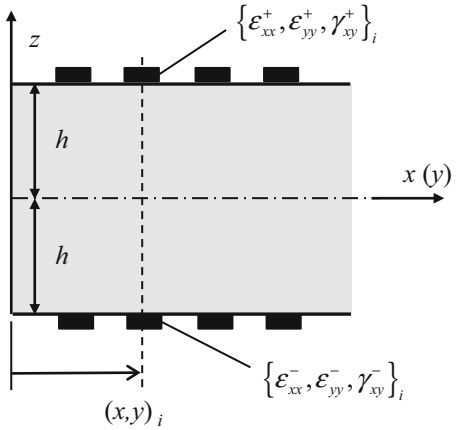

Fig. 2 Strain gauge instrumentation

$$\Phi^e_k \equiv \int_{A^e} \varepsilon^2_{k(i)}(\mathbf{u}^e)dA \tag{10}$$

where A^e is the element area.

The weighting coefficients are $\{w^e_k\} = \{\lambda^e_1, \lambda^e_2, \lambda^e_3, t^2\lambda^e_4, t^2\lambda^e_5, t^2\lambda^e_6, \lambda^e_7, \lambda^e_8\}$, where λ^e_k $(k = 1,\ldots, 8)$ are dimensionless, positive constants (see Sect. 3). In general, when only few strain sensors are available, some elements may not have any strain data. In this case, Eq. (10) is used instead of Eq. (5) for all the terms in the functional ($k = 1,\ldots, 8$). For these elements, small values are used for $\lambda^e_k(k = 1,\ldots, 8)$ compared to the values used for the elements that possess strain data (refer to [29] and Sect. 3).

3 Shape sensing of a composite stiffened panel

The static and dynamic responses of a CFRP (Carbon-Fiber Reinforced Plastic) stiffened plate are herein determined using numerical surface strains and the inverse Finite Element Method under: (a) a distributed static load, (b) a time-varying distributed load and (b) a thermal load.

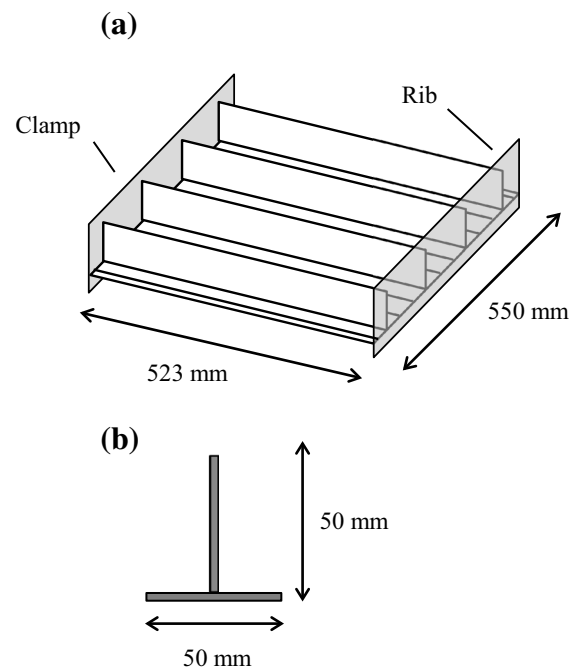

Fig. 3 Geometry of **a** stiffened panel and **b** T-beam stiffener cross-section

The panel is 523 mm long and 550 mm wide. The four T-beam stiffeners have dimensions 50 × 50 mm (Fig. 3). The skin panel is made of a 16-layer Carbon-Epoxy composite laminate having symmetric, angle-ply stacking sequence, corresponding to $[45, -45, 0, 90]_{2s}$. The stiffeners are made of 18 layers oriented as $[45, -45, 0, 0, 90, 45, -45, 0, 0]_s$. The thickness of each lamina is 0.1875 mm; thus, the skin is thick 3 mm, while the wall-thickness of the stiffeners is 3.375 mm. The material properties of the single lamina, made of Carbon-Epoxy unidirectional composite, are listed in Table 1. One end of the plate is clamped, whereas a rigid body constraint is applied to the other end, to simulate the presence of a rib (Fig. 3).

To obtain the input strain data, linear elastic analyses were carried out using a high-fidelity NASTRAN model. The model consists of 10,196 QUAD4 shell elements and one Rigid Body Element, RBE2, connecting the nodes on the edge where the rib is ideally located (see Fig. 4). The T-beam stiffeners are linked to the skin panel with a node-to-node rigid connection, simulating a perfect bond. The same analyses serve as a reference to verify the accuracy of the iFEM displacement solutions. Considering the high-fidelity of the NASTRAN model, the strains were taken at the nodes of the mesh, instead of the Gaussian points of the elements.

The strain-sensor configuration here tested is composed of uniaxial strain-sensors, aligned within each bay, on the top and bottom surfaces of the skin, as depicted in Fig. 5. The iFEM mesh consists of 720 triangular, inverse elements and one Rigid Body Element (RBE); the strain sensors are located at the centroids of the inverse elements (see Fig. 5). Since a limited set of measurement point is used, i.e., strains are not measured within each inverse element, the weighted least squares approach is used (see Sect. 2). Particularly, when the experimental estimate of a strain measure is not available, the weighting coefficients are defined as $\lambda_k^e = 10^{-4}$, $(k = 1, \ldots, 6)$, whereas $\lambda_7^e = \lambda_8^e = 10^{-2}$ is used for all the elements (refer to [29]).

The present discretization and strain-sensor configuration represents a good compromise between the number of elements needed to satisfactorily approximate the deformed shape of the panel and the number of measurement points. In fact, increasing the number of elements along the main direction of the stiffeners would require a higher number of strain measurements. On the other hand, the number of inverse elements should be adequate to correctly approximate the deformed shape of the panel. A too coarse mesh would result in a rough approximation of the actual deformed shape.

3.1 Static loading

A distributed pressure has been applied to the skin of the panel, having a linear distribution. Particularly, the pressure is constant along the direction of the stiffeners while it varies linearly within the width of the panel as $p_z = 1.5 \times 10^{-2} - y/55000$ N/mm^2, with $y \in [0, 550]$. As a result, both bending and torsion are observed. Figure 6 shows the deformed shapes computed by high-fidelity direct FE analyses and by inverse FEM using the low-fidelity mesh of inverse elements. The direct and inverse FEM analyses compare very well across the entire panel, with the maximum deflection being predicted with an error of about 1.3 %.

3.2 Dynamic loading

The distributed pressure defined in Sect. 3.1 is now used as a time-varying load. Particularly, a harmonic

Table 1 Mechanical properties of Carbon-Epoxy unidirectional (UD) composite

	Symbol	Units	Carbon–Epoxy UD
Young's modulus 0°	$E_1^{(k)}$	GPa	135
Young's modulus 90°	$E_2^{(k)}(=E_3^{(k)})$	GPa	10
In-plane shear modulus	$G_{12}^{(k)}(=G_{13}^{(k)})$	GPa	5
Transverse shear modulus	$G_{23}^{(k)}$	GPa	5
In-plane Poisson's ratio	$\nu_{12}^{(k)}(=\nu_{13}^{(k)})$	–	0.3
Thermal exp. coefficient 0°	α_1	Strain/K	−0.3
Thermal exp. coefficient 90°	α_2	Strain/K	28
Density	ρ	g/cm^3	1.6

Fig. 4 NASTRAN model

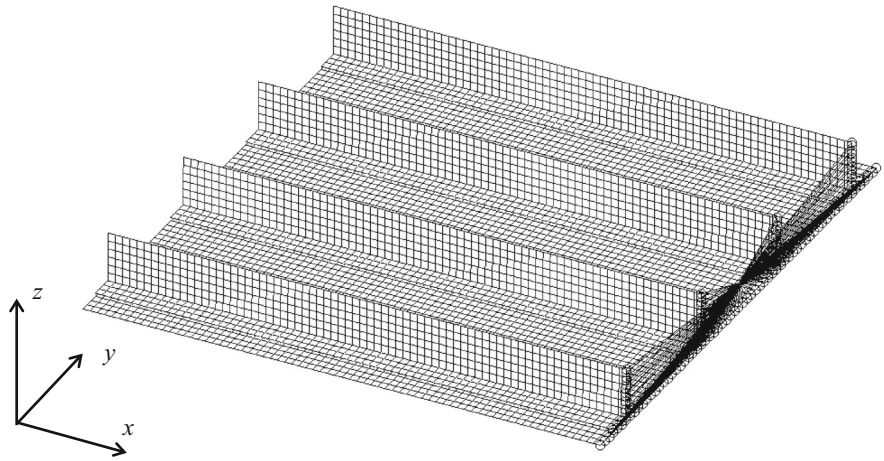

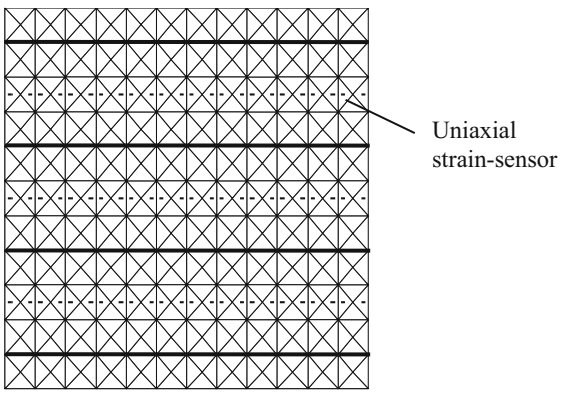

Fig. 5 iFEM mesh and uniaxial strain-sensor distribution (strain sensors on the top and bottom surfaces of the skin)

vertical pressure $\bar{p}_z(t)$ (where t denotes time), acting on the skin of the panel with the frequency $f_0 = 30$ Hz, has the form $\bar{p}_z(t) = p_z \sin(2\pi f_0 t)$. For the NASTRAN analysis a critical damping ratio of 5 % has been defined; note that for the inverse analysis no inertial/damping characteristics are required. Figure 7 displays the deflection at the point of maximum displacement, that is, $x = 523$ and $y = 0$, evaluated with both iFEM and NASTRAN, in the first tenth of a seconds. It is evident that iFEM is able to predict the dynamic response of the composite panel with a great accuracy, in both transient and steady-state regimes. Particularly, the maximum/minimum displacement is predicted with an error of about 2.5 %.

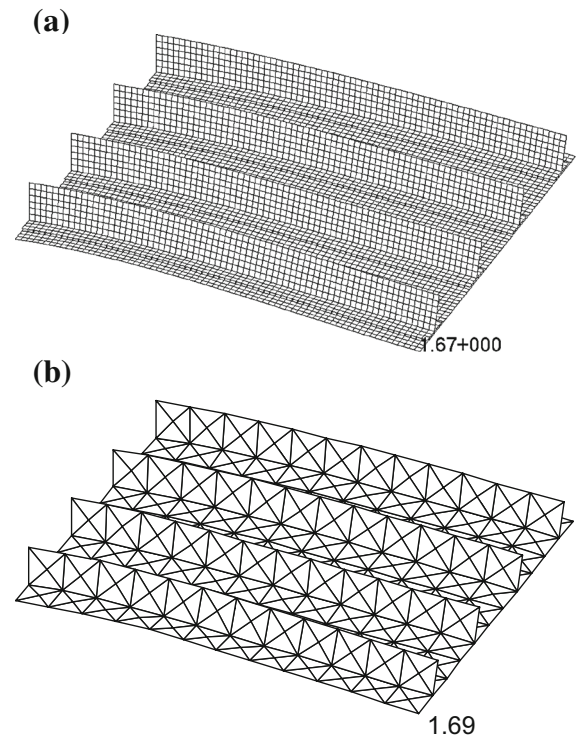

Fig. 6 Deformed shape of the panel under static distributed pressure: **a** NASTRAN evaluated deflection and **b** iFEM prediction

3.3 Thermal loading

A thermal load has been applied by imposing a uniform positive temperature variation, $\Delta T = 30°$ C.

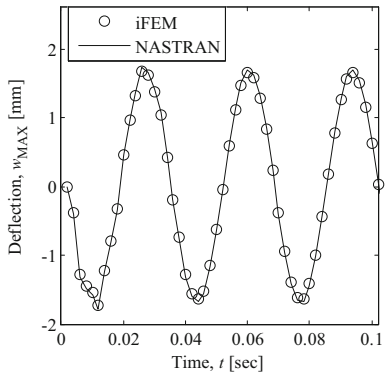

Fig. 7 Comparison of the deflection evaluated with iFEM at the point of maximum displacement ($x = 523$, $y = 0$) to the NASTRAN solution

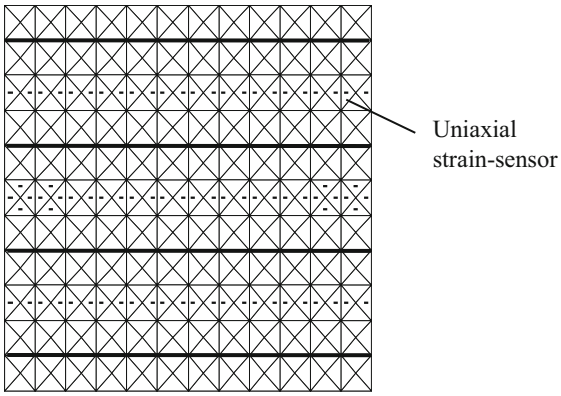

Fig. 8 iFEM mesh and strain-sensor distribution for the thermal loading (uniaxial strain-sensors on the *top* and *bottom* surfaces of the skin)

At first, the same strain-sensor configuration of Fig. 5 was used but no satisfactory results were obtained. It has to be remarked that a thermal load applied to a multilayered CFRP structure induces complex strain distributions and thus higher-fidelity discretizations of inverse elements and/or a larger number of strain data are needed to accurately reconstruct the deformed shape. For this purpose, a slightly different strain-sensor configuration has been defined by adding eight uniaxial strain sensors on the top surface and eight sensors on the bottom surface of the skin, distributed within the central bay (see Fig. 8). Results obtained with the inverse mesh and strain-sensor configuration of Fig. 8 are compared to NASTRAN solution in Fig. 9. The two solutions are found to be in good agreement including maximum deflection value (refer

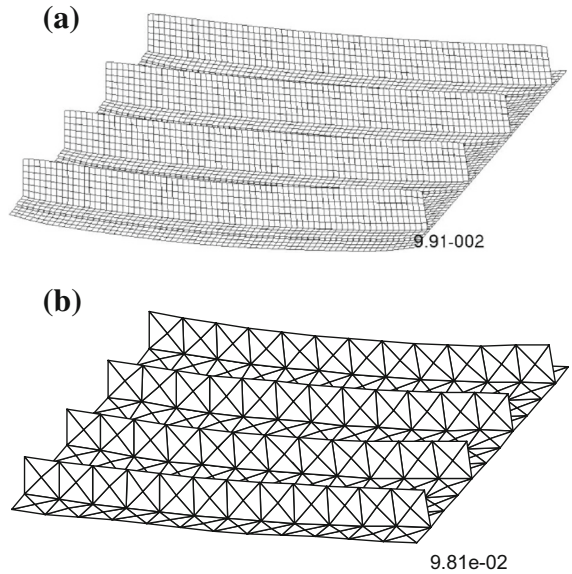

Fig. 9 Deformed shape of the panel subjected to the thermal load: **a** NASTRAN evaluated deflection and **b** iFEM prediction

to Fig. 9). The inverse Finite Element method, which is based on strain–displacement relationships only, is proven to be effective in predicting deformed shape also when structural deformation is induced by temperature changes.

4 Sensitivity to input uncertainties

Since the experimental values of surface strains are the key input quantities, it is particularly important to study the accuracy of the predicted displacements under the influence of errors in the measured strains. Such inherent errors include those due to measurements themselves and also uncertainty in strain-gauge positions. Thus, normally distributed errors have been independently added to the strains computed from the NASTRAN FE analyses. These strains have zero mean value and three standard deviations equal to $3\sigma = 5$ % of the NASTRAN strains, i.e., about 99.7 % of the errors are within the interval (-5 %; $+5$ %). The probability density function of the predicted maximum deflection has been evaluated with a Monte-Carlo simulation, consisting of 10^3 trial points (Fig. 10). The maximum deflection value is predicted within -5 % and $+5$ % error for the 93 % of the cases.

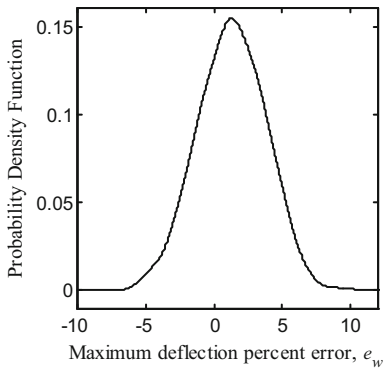

Fig. 10 Probability density function of the percent error on maximum deflection, $e_w \equiv 100(w_{\max}/w_{\max}^{NASTRAN} - 1)$

5 Conclusions

In this paper, the inverse Finite Element Method (iFEM) has been used to reconstruct both static and dynamic response of a composite stiffened panel from discrete strain data. This type of structure is commonly employed in aerospace, naval, and civil engineering applications. Despite of having numerous advantages, composite structures may experience such modes of failure as delamination and impact damage, and these can affect their load carrying capabilities. For this purpose, the knowledge of structural displacements can be used to evaluate the strain and stress fields for assessing real-time internal loads and structural integrity. Moreover, monitoring of the deformed shape is fundamental for providing feedback to the actuation and control systems of morphing structures.

An overview of the inverse Finite Element Method (iFEM) has been presented highlighting the essential features. Utilizing surface strain measurements, iFEM enables reconstruction of the three-dimensional displacement field of general built-up shells, trusses, beams, and frames under both static and dynamic loading conditions. The basic concept and governing equations of iFEM have been reviewed. The formulation of a three-node, triangular inverse elements for the shape sensing of shell and plate structures has been discussed. The inverse Finite Element method has then been used to reconstruct the deformed shape of a composite stiffened panel, subjected to static, dynamic and thermal loads. The surface-strain measurements used in the iFEM analyses have been numerically generated by way of high-fidelity FE models. The predicted deformed shape resulted to be in excellent agreement with the reference high-fidelity FE results.

Finally, it should be once again noted that, for the purpose of shape-sensing analysis, iFEM does not require the knowledge of applied loading, elastic or inertial material properties, or the damping characteristics of the structure. As it has been demonstrated, a well-designed iFEM-based structural model, even in the presence of relatively coarse measured strain-data and stochastically distributed errors, can lead to very accurate shape sensing predictions of practical importance. Particularly, being the prediction error very small, little changes in the structures, due to defects or damages, may be detectable. Future work should focus on determining the range of validity of the present method for damage detection. The main advantages of using iFEM for Structural Health Monitoring (SHM) are that, the whole structure can be monitored with a reduced set of measured strains in every material point, also far from sensor locations.

References

1. Abrate S (1998) Impact on composite structures. Cambridge University Press, Cambridge
2. Takeda S, Minakuchi S, Okabe Y, Takeda N (2005) Delamination monitoring of laminated composites subjected low-velocity impact using small-diameter FBG sensors. Compos A 36:903–908
3. Greenhalgh E, Meeks C, Clarke A, Thatcher J (2003) The performance of post-buckled CFRP stringer-stiffened panels containing defects and damage. In: Proceedings of the 44th AIAA/ASME/ASCE/AHS/ASC structures, structural dynamics, and materials conference, AIAA 2003-1680
4. Takeda S-I, Aoki Y, Nagao Y (2012) Damage monitoring of CFRP stiffened panels under compressive load using FBG sensors. Compos Struct 94:813–819
5. Bray DE, McBride D (1992) Nondestructive testing techniques. Wiley, New York
6. Jones R, Galea S (2002) Health monitoring of composite repairs and joints using optical fibres. Compos Struct 58:397–403
7. Staszewski WJ, Boller C, Tomlinson GR (2004) Health monitoring of aerospace structures-smart sensor technologies and signal processing. Wiley, New York
8. Baroth E, Powers WT, Fox J, Prosser B, Pallix J, Schweikard K, Zakrajsek J (2001) IVHM (integrated vehicle health management) techniques for future space vehicles. In: Proceedings of the 37th AIAA/ASME/SAE/ASEE joint propulsion conference exhibit, AIAA 2001-3523
9. Paris DE, Trevino LC, Watson MD (2005) A framework for integration of IVHM technologies for intelligent integration for vehicle management. In: Proceedings of the 2005 IEEE aerospace conference, pp 3843–3852

10. Staszewski WJ, Boller C, Tomlinson GR (2004) Health monitoring of aerospace structures-smart sensor technologies and signal processing. Wiley, Newyork
11. De Stefano M, Gherlone M, Mattone M, Di Sciuva M, Worden K (2015) Optimum sensor placement for impact location using trilateration. Strain 51:89–100
12. Worden K, Staszewski WJ (2000) Impact location and quantification on a composite panel using neural networks and genetic algorithms. Strain 36:61–68
13. Quach CC, Vazquez SL, Tessler A, Moore JP, Cooper EG, Spangler JL (2005) Structural anomaly detection using fiber optic sensors and inverse Finite Element Method. In: Proceedings of AIAA guidance, navigation, and control conference and exhibit, AIAA 2005-6357
14. Derkevorkian A, Masri SF, Alvarenga J, Boussalis H, Bakalyar J, Richards L (2013) Strain-based deformation shape-estimation algorithm for control and monitoring applications. AIAA J 51:2231–2240
15. Hopkins MA, Truss JM, Lockyer AJ, Alt K, Kinslow R, Kudva JN (1997) Smart skin conformal load bearing antenna and other smart structures developments. In: Proceedings of the 38th AIAA/ASME/ASCE/AHS/ASC, structures, structural dynamics and materials conference, pp 521–530
16. Yin W, Fu T, Liu J, Leng J(2009) Structural shape sensing for variable camber wing using FBG sensors. In: Proceedings of SPIE 7292, Sensors and smart structures technologies for civil, mechanical, and aerospace systems, 72921H
17. Ko WL, Richards WL, Fleischer VT (2009) Applications of the Ko displacement theory to the deformed shape predictions of the doubly-tapered Ikhana wing. NASA technical report, NASA/TP-2009-214652
18. Gopinathan M, Pajunen GA, Neelakanta PS, Arockaisamy M (1995) Recursive estimation of displacement and velocity in a cantilever beam using a measured set of distributed strain data. J Intell Mater Syst Struct 6:537–549
19. Davis MA, Kersey AD, Sirkis J, Friebele EJ (1996) Shape and vibration mode sensing using a fiber optic Bragg grating array. Smart Mater Struct 5:759–765
20. Jones RT, Bellemore DG, Berkoff TA, Sirkis JS, Davis MA, Putnam MA, Friebele EJ, Kersey AD (1998) Determination of cantilever plate shapes using wavelength division multiplexed fiber Bragg grating sensors and a least-squares strain-fitting algorithm. Smart Mater Struct 7:178–188
21. Glaser R, Caccese V, Shahinpoor M (2012) Shape monitoring of a beam structure from measured strain or curvature. Exp Mech 52:591–606
22. Foss GC, Haugse ED (1995) Using modal test results to develop strain to displacement transformations. In: Proceedings of the 13th international modal analysis conference, pp 112–118
23. Pisoni AC, Santolini C, Hauf DE, Dubowsky S (1995) Displacements in a vibrating body by strain gauge measurements. In: Proceedings of the 13th international modal analysis conference, pp 119–125
24. Bogert PB, Haugse ED, Gehrki RE (2003) Structural shape identification from experimental strains using a modal transformation technique. In: Proceedings of the 44th AIAA/ASME/ASCE/AHS structures, structural dynamics and materials conference, AIAA 2003-1626
25. Kang LH, Kim DK, Han JH (2007) Estimation of dynamic structural displacements using fiber Bragg grating strain sensors. J Sound Vib 305:534–542
26. Lively PS, Atalla MJ, Hagood NW (2001) Investigation of filtering techniques applied to the dynamic shape estimation problem. Smart Mater Struct 10:264–272
27. Tessler A, Spangler JL (2005) A least-squares variational method for full-field reconstruction of elastic deformations in shear-deformable plates and shells. Comput Method Appl M 194:327–339
28. Tessler A, Spangler JL (2004) Inverse FEM for full-field reconstruction of elastic deformations in shear deformable plates and shells. In: Proceedings of the 2nd European workshop on structural health monitoring, pp 83–92
29. Tessler A, Spangler JL, Mattone M, Gherlone M, Di Sciuva M (2011) Real-time characterization of aerospace structures using onboard strain measurement technologies and inverse Finite Element Method In: Proceedings of the 8th international workshop on structural health monitoring, pp 981–988
30. Gherlone M, Cerracchio P, Mattone M, Di Sciuva M, Tessler A (2012) Shape sensing of 3D frame structures using an inverse Finite Element Method. Int J Solids Struct 49:3100–3112
31. Gherlone M, Cerracchio P, Mattone M, Di Sciuva M, Tessler A (2014) Inverse Finite Element Method for beam shape sensing: theoretical framework and experimental validation. Smart Mater Struct 23:045027